

Article

Multi-Mode Shape Control of Active Compliant Aerospace Structures Using Anisotropic Piezocomposite Materials in Antisymmetric Bimorph Configuration

Xiaoming Wang ^{1,*} , Xinhan Hu ² , Chengbin Huang ² and Wenya Zhou ²¹ School of Mechanical and Electrical Engineering, Guangzhou University, Guangzhou 510006, China² Liaoning Provincial Key Laboratory of Aerospace Advanced Technology, School of Aeronautics and Astronautics, Dalian University of Technology, Dalian 116024, China; huxinhan@mail.dlut.edu.cn (X.H.); 904368073@mail.dlut.edu.cn (C.H.); zwy@dlut.edu.cn (W.Z.)

* Correspondence: wangxm@gzhu.edu.cn

Abstract: The mission performance of future advanced aerospace structures can be synthetically improved via active shape control utilizing piezoelectric materials. Multiple work modes are required. Bending/twisting mode control receives special attention for many classic aerospace structures, such as active reflector systems, active blades, and compliant morphing wings. Piezoelectric fiber composite (Piezocomposite) material features in-plane anisotropic actuation, which is very suitable for multiple work modes. In this study, two identical macro-fiber composite (MFC) actuators of the F1 type were bonded to the base plate structure in an “antisymmetric angle-ply bimorph configuration” in order to achieve independent bending/twisting shape control. In terms of the finite element model and homogenization strategy, the locations of bimorph MFCs were determined by considering the effect of trade-off control capabilities on the bending and twisting shapes. The modal characteristics were investigated via both experimental and theoretical approaches. The experimental tests implied that the shape control accuracy was heavily reduced due to various uncertainties and nonlinearities, including hysteresis and the creep effect of the actuators, model errors, and external disturbances. A multi-mode feedback control law was designed and the experimental tests indicated that synthetic (independent and coupled) bending/twisting deformations were achieved with improved shape accuracy. This study provides a feasible multi-mode shape control approach with high surface accuracy, especially by employing piezocomposite materials.

Keywords: shape control; macro-fiber composites; bending; twisting; experimental validation; control system



Citation: Wang, X.; Hu, X.; Huang, C.; Zhou, W. Multi-Mode Shape Control of Active Compliant Aerospace Structures Using Anisotropic Piezocomposite Materials in Antisymmetric Bimorph Configuration. *Aerospace* **2022**, *9*, 195. <https://doi.org/10.3390/aerospace9040195>

Academic Editor: Gianpietro Di Rito

Received: 21 February 2022

Accepted: 2 April 2022

Published: 6 April 2022

Publisher's Note: MDPI stays neutral with regard to jurisdictional claims in published maps and institutional affiliations.



Copyright: © 2022 by the authors. Licensee MDPI, Basel, Switzerland. This article is an open access article distributed under the terms and conditions of the Creative Commons Attribution (CC BY) license (<https://creativecommons.org/licenses/by/4.0/>).

1. Introduction

Owing to the increasingly stringent requirements for industrial equipment, particularly for the aerospace fields, smart devices and structures are receiving increasing attention to improve the synthetic or specific performances of systems [1–3]. Amongst these devices and structures, piezoelectric materials are the most widely used actuators or sensors for various applications, including shape control, vibration suppression, and health monitoring [4,5]. Active structures integrated with piezoelectric materials can change their shape or profile to enhance the accuracy and adaptability of the system via an active control approach. Some classic instances are active reflector systems, active blades, and compliant morphing wings [6–8].

Structural shape control utilizing piezoelectric materials is mainly implemented for two purposes: (1) To correct the shape error of the structure due to manufacturing error or external disturbance; and (2) to provide active shape control for morphing applications with a specific purpose, such as mechanically reconfigurable reflectors (MRRs) and compliant morphing wings. For reflector systems, particularly the large deployable antennas

that will be used in the future, high surface precision is required to maintain position accuracy; however, surface errors are induced by many factors, including assembly error, deployment accuracy, environmental loads, or mechanical creep [9]. Active shape control has been proven as a feasible approach to correct reflector surface errors and ensure high shape accuracy. Bradford [6] investigated active reflector systems actuated by macro-fiber composite (MFC) arrays to correct thermally induced deformations and manufacturing errors. Hill [10] investigated the feasibility of using distributed polyvinylidene fluoride actuators in the active control of a large-scale reflector under thermal load. Wang [11] used PZT actuators to adjust the surfaces of flexible cable net antennas using quadratic criteria. Song [12] presented an experimental validation of a PZT-actuated CFRP reflector using a closed-loop iterative shape control method based on the influence coefficient matrix. In addition to modifying the shape error, piezoelectric actuators can also be used for mechanically reconfigurable reflectors that can actively reshape its surface according to the purpose, such as modifying the service coverage. Tanaka and Hiraku [13,14] developed MRR prototypes with six spherical piezoelectric actuators. Shao [7] designed a mechanically reconfigurable reflector using 30 piezoelectric inchworm actuators and presented a distributed time-sharing control strategy to minimize the size and power of the MRR system. In the aviation field, piezoelectric materials are often used for the active shape control of both fixed and rotating wings. Monner [15,16] developed “active twist blades” and used MFCs for twist actuation. Li [17] presented an experimental validation of the feasibility of using piezoelectric actuators to improve rolling power at all dynamic pressures via elastic wing twist. In the last decade, the use of piezocomposite materials, especially MFCs, in compliant morphing wing designs has been broadly investigated. Bilgen [8,18,19] devoted many studies towards the design, optimization, and wind-tunnel testing of MFC-actuated compliant morphing wings, and implemented the flight control of micro-air-vehicles (MAVs). LaCroix [20] used MFCs to deform the surface of the forward-swept thin, compliant composite wings of MAVs. Molinari [21] designed a three-dimensional adaptive compliant wing with embedded MFCs and presented aero-structural optimization. These prior works demonstrated that MFCs produce a large actuation effect to deform compliant structures. Compared with conventional hinged, discrete-control surfaces, MFC-actuated morphing wings perform with lower drag and offer more efficient production of control forces and moments.

For future smart structures, multiple work modes, such as bending, twisting, and expansion, will need to be controlled in many circumstances. Concerning some common structures, such as beams or plates, bending deformations are mostly considered due to their larger deformation magnitude and lower inherent frequencies. Twisting deformation and corresponding control issues receive specific attention in many fields, particularly for flexible wing structures. Twist morphing is one of the most popular categories of morphing wings and has resulted in a large number of wind-tunnel and flight tests in aircraft [1]. Some other instances are rotating blades, solar panels, and robot arms, whose behaviors also consist of both bending and twisting modes.

In a piezo-actuation context, in-plane polarized, anisotropic piezocomposite materials are the natural choices for multiple work modes including bending/twisting shape control. Conventional piezoceramics, such as lead zirconium titanate (PZT), are typically capable of large actuation forces; however, they have some limitations, such as small strains and low flexibility [22]. In addition, traditional actuators with through-the-thickness poling possess transverse isotropy in the plane and cannot supply sufficient twisting actuation moment [23]. Piezocomposite materials have emerged as the new class of hybrid materials; they consist of piezoelectric fiber reinforcements embedded in the epoxy matrix and interdigitated electrodes, so they can provide a wide range of effective material properties, good conformability, and strength integrity [24,25]. Piezocomposite materials can utilize the d_{33} piezoelectric effect in the direction of PZT fibers, which is larger than the d_{31} piezoelectric effect of conventional piezoelectric actuators [26]. In particular, piezocomposite actuator patches feature anisotropic actuation effects, which makes it possible to expand their work

modes by designing specific PZF fiber orientations [15,23,27–29]. For the MFCs used in this study, three work modes (expansion, bending, and torsion), were realized and, of course, the appropriate actuator types and configurations were chosen for specific modes. Smart Material Corporation [30] provides two types of standard MFC actuator patch that utilize the d_{33} effect: P1 types with 0° fiber orientation and F1 types with 45° fiber orientation. The P1-type actuators are mainly used for the bending control of structures and the F1-type actuators are used for twisting control. In addition to unimorph-configuration actuators, piezocomposite actuators in bimorph configuration are commonly adopted to enhance control authority [21,31–34]. Bilgen [31] designed a lightweight high-voltage electronic circuit for MFC bimorphs and remedied the situations in which the MFCs had an asymmetry range in the positive and negative voltage directions. In the authors' previous studies, piezocomposite materials in "antisymmetric angle-ply bimorph configuration" were presented for the bending/twisting shape control of plate-like flexible wing structures [35,36]. The actuator optimizations (in unimorph or bimorph configuration) [37,38] and structure/actuator-integrated designs [39] for such piezocomposite-actuated structures were also presented. In addition to theoretical investigations, experimental validations are also presented in this paper to demonstrate the feasibility of bimorph MFCs for bending/twisting mode control and real-time control systems.

The primary aim of this paper is to present both theoretical and experimental investigations of the control performance of anisotropic piezocomposite actuators in synthetic (independent and coupled) bending/twisting shape control. In this study, two MFCs of the F1 type in bimorph configuration were used for the shape control of a cantilever aluminum plate. The two identical actuators were orientated at $\pm 45^\circ$ from the front and backside surfaces, respectively. Thus, in ideal situations, the same potential would induce pure twisting, whereas the opposite potential would cause pure bending. The finite element method was applied to model the system and optimize the actuators' locations. An experimental setup was built for the MFC-actuated flexible plate, whose deformation was measured using two laser displacement sensors. A feedback closed-loop control law was designed to improve the shape control accuracy when it was subjected to uncertainties and nonlinearities. Finally, the multi-mode control scheme was experimentally verified using pure bending, twisting, and coupled bending/twisting shape control.

2. Model Formulation

2.1. MFC-Actuated Plate Structures

The active structure in this study is characterized by means of a cantilever aluminum plate, as shown in Figure 1. Two identical MFC patches of M8557-F1 type, which were produced by Smart Material Corp., Sarasota, FL, US, were symmetrically glued to the front and backside surfaces of the base plate, respectively. This type of F1 MFC actuator features a 45° fiber orientation with respect to its length direction. Practically, due to the opposite surfaces, the actual fiber orientations for the two actuators were -45° and 45° with respect to the global x -axis, respectively. Note that the electrodes of the actuator always remained perpendicular to the fiber orientation. That is to say, the actuators were in the so-called "antisymmetric angle-ply bimorph configuration", which offers several unique advantages for active shape control. First and foremost, independent bending or twisting deformations could be produced using the opposite or the same potential, respectively; the detailed descriptions are given in the subsequent subsections. Compared with unimorph configuration, larger actuation ability and control authority could be produced. Furthermore, the elastic axis of the base plate is unchanged under bimorph configuration, which may be beneficial for flexible wings [35,36]. Table 1 lists the geometric and material properties (theoretical value) of the base plate and MFC actuators.

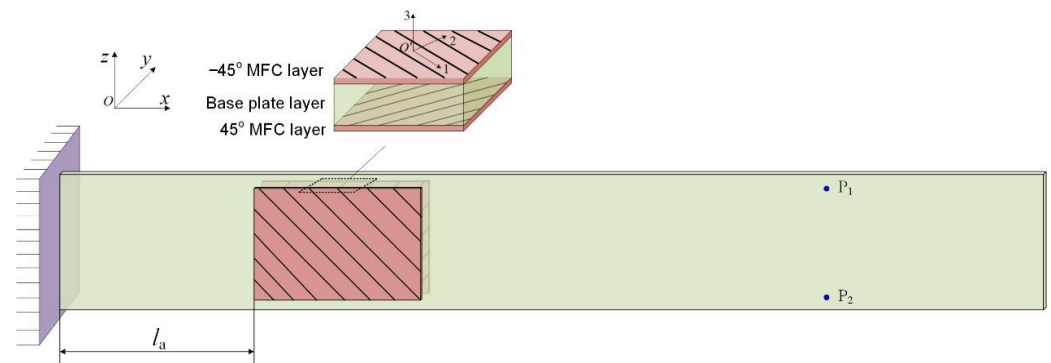


Figure 1. Schematics of the MFC-actuated compliant plate structure.

Table 1. The geometric and material properties (theoretical value) of plant.

Parameters	Values	
	Base Plate	MFC Actuator [30]
Length (mm)	500	85 (active area)
Width (mm)	64.5	57 (active area)
Thickness (mm)	1	0.3
Modulus of elasticity (GPa)	70.3	30.34, 15.86
Poisson's ratio	0.345	0.31, 0.16
Density (kg/m ³)	2700	5400
Actuator location		100 mm from the root
Measurement point locations		105 mm from the tip
Piezoelectric constants (m/V)		400×10^{-12} , -170×10^{-12}
Fiber orientations (deg)		$\pm 45^\circ$
Electrode spacing		0.5 mm

Because the laser displacement sensors were used to measure the elastic deformation, two measurement points, which were symmetrical relative to the midline, as shown in the figure, were chosen to represent the bending and twisting deformations. The optimization of the locations of the MFC actuators is described in the following sections.

2.2. Finite Element Model

A mathematical model is commonly needed to predict the behaviors of systems and can also be used for model-based control system design. The finite element method was used in this study to model the piezocomposite-actuated plate. Figure 2 depicts the finite element model. Quadrilateral plate elements were adopted to discretize the structure. The key issue was to model the MFC actuator, which is a hybrid, layered material that consists of a rectangular cross-section, unidirectional piezoceramic fibers, the epoxy matrix, Kapton, and interdigitated electrodes [40]. Due to the complexity of MFCs, a homogenization strategy was adopted; thus, the actuator could be modeled in the form of homogenized orthotropic materials with arbitrary PZT fiber orientations, as well as composite materials [41,42]. Moreover, the local mass and stiffness change induced by the bonded patch was determined through composite laminate theory. Detailed descriptions of the FEM approach have been presented in [38,39]. For the sake of simplicity, the final governing equations are obtained and written as

$$M\ddot{x} + Kx = B_u u \quad (1)$$

where x is the vector of the nodal displacements. The matrices M and K denote the mass matrix and stiffness matrix, which are assembled as $M = M_b + M_p$ and $K = K_b + K_p$, respectively, where subscripts b and p denote the contribution of the base plate layer and piezocomposite layers, respectively. $u = [u_1 \ u_1]^T$ is the vector of the applied voltages. B_u is the coefficient matrix, which depends on the actuator locations.

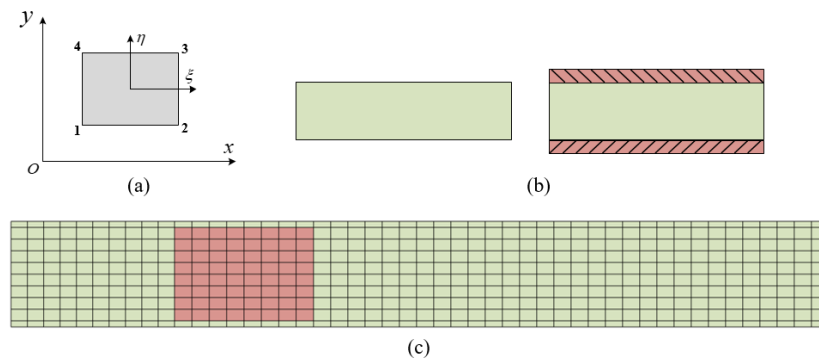


Figure 2. Finite element model of the piezo-actuated plate: (a) Quadrilateral plate element; (b) cross-sections of the elements; (c) meshes of the structure.

The deflections of the two measurement points P_1 and P_2 are given by

$$\begin{aligned} w_{P_1} &= C_{P_1} \mathbf{x} \\ w_{P_2} &= C_{P_2} \mathbf{x} \end{aligned} \tag{2}$$

where C_{P_1} and C_{P_2} are the output matrices, which depend on the measurement locations of the laser sensors.

2.3. Actuator Position Optimization

It is an important issue to determine how to efficiently use piezoelectric capabilities to their fullest extent in active shape control. Accordingly, the locations of the actuators must be optimized before performing experiments. Extensive research on the optimal placement of piezoelectric actuators for structural control has also been carried out. Some detailed literature reviews on this topic can be found in [43–45]. The authors have also presented the optimization approach for the anisotropic piezocomposite actuators by considering the PZT fiber orientations as well as the distributed positions [37–39]. However, due to the fixed size and fiber orientation of M8557-F1-type MFC actuators, only the position of the actuators in the length direction can be designed. Thus, the best position can be chosen via traversal simulations, which is not time-consuming. Moreover, the influence of the actuator’s position on shape control ability can also be reflected in this way. Therefore, only one design variable is concerned and given as

$$l_a \in [0, L - l] \tag{3}$$

where l_a is the distance from the plate root to the left edge of the active area of the MFC, as shown in Figure 1. Note that, to facilitate the theoretical simulation, only the active area of MFC is considered. The values L and l denote the length of the base plate and actuator, respectively.

Because both bending and twisting are concerned, two corresponding criteria are used to evaluate the shape control capabilities and given by

$$J_1 = |w_{P_1}|, \mathbf{u} = [500, -500]^T \tag{4}$$

$$J_2 = |\alpha|, \mathbf{u} = [500, 500]^T \tag{5}$$

$$\alpha = \arcsin \frac{w_{P_1} - w_{P_2}}{|P_1 P_2|} \approx \frac{w_{P_1} - w_{P_2}}{|P_1 P_2|} \tag{6}$$

where $|P_1 P_2|$ denotes the distance between two measurement points.

The variations of J_1 and J_2 with l_a are shown in Figure 3a, respectively. It was found that the bending deformation decreased monotonically with the length position of the actuator, i.e., the best position was the root area, as depicted in Figure 3(b.1). However, it

was preferable to place the actuator in the area of 0.1 m~0.35 m so as to obtain enhanced twisting control capability, while the largest twisting deformation occurred in $l_a = 0.22$ m, as depicted in Figure 3(b.2). Hence, the area of the shaded part in Figure 3a is a kind of Pareto optimal area, in which any point could be viewed as an acceptable location. Therefore, after considering the trade-off in control authority between the bending and torsional modes, we chose a final position of $l_a = 0.1$ m. The above discussions explain why we placed the MFC actuators in this position.

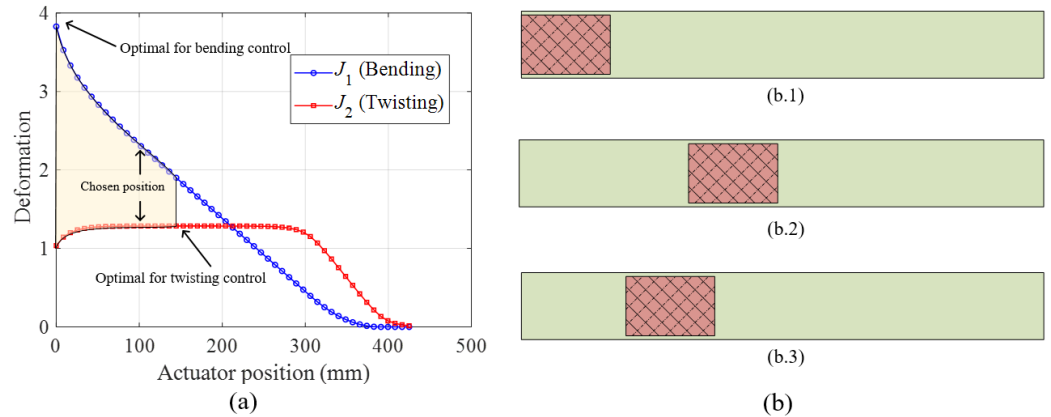


Figure 3. Variations in the bending and twisting deformations with the position of the actuator: (a) The variations in the bending and twisting deformations with actuator position; (b.1) the best position for bending control; (b.2) the best position for twisting control; (b.3) the chosen position for multi-mode shape control.

2.4. Theoretical Bending/Twisting Shape Control

As previously mentioned, the primary aim of this study was to achieve synthetic (independent and coupled) bending and twisting shape control. To theoretically demonstrate the bending/twisting control principle, the deformation configuration of the plate under the actuation of a single MFC is presented in Figure 4. The results demonstrate that both bending and twisting deformations were produced under the actuation of a single F1-type MFC. For the MFC1 that was bonded on the front side of the plate, the deflection amplitude of the lower measurement point was larger than the upper measurement $w_{P_1, MFC1}$. By contrast, the deformation trend produced by the MFC2 alone was opposite in not only the direction but also in the relations between w_{P_1} and w_{P_2} , i.e.,

$$\begin{aligned} |w_{P_1, MFC1}| &< |w_{P_2, MFC1}| \\ |w_{P_1, MFC2}| &> |w_{P_2, MFC2}| \end{aligned} \tag{7}$$

In ideal situations, the following relation exists:

$$\begin{aligned} |w_{P_1, MFC1}| &= |w_{P_2, MFC2}| \\ |w_{P_1, MFC2}| &= |w_{P_2, MFC1}| \end{aligned} \tag{8}$$

Consequently, employing this bimorph configuration, the two actuators could be polarized in the same direction for twisting deformation and polarized in opposite directions for bending deformation. The voltage input applied for the front and backside actuators are defined as u_1 and u_2 , respectively. By applying the same voltages (i.e., $u_1 = u_2$), pure moments of torque are generated, while the bending moments are canceled out. On the other hand, pure bending deformation can be achieved by using the opposite voltages ($u_1 = -u_2$). Of course, a combination of bending and twisting deformations can be performed by designing the two voltages. In a practical context, for any two voltages, the decomposition is given as

$$\begin{aligned} u_1 &= u_s + u_o \\ u_2 &= u_s - u_o \end{aligned} \tag{9}$$

where $u_s = \frac{u_1+u_2}{2}$, $u_o = \frac{u_1-u_2}{2}$ are the voltage components for twisting and bending deformation, respectively. The subscripts “s” and “o” correspond to the same and the opposite components. Figure 5 visualizes the voltage distribution for the two MFC actuators and Figure 6 shows the bending and twisting deformation obtained from the simulation by applying different voltages.

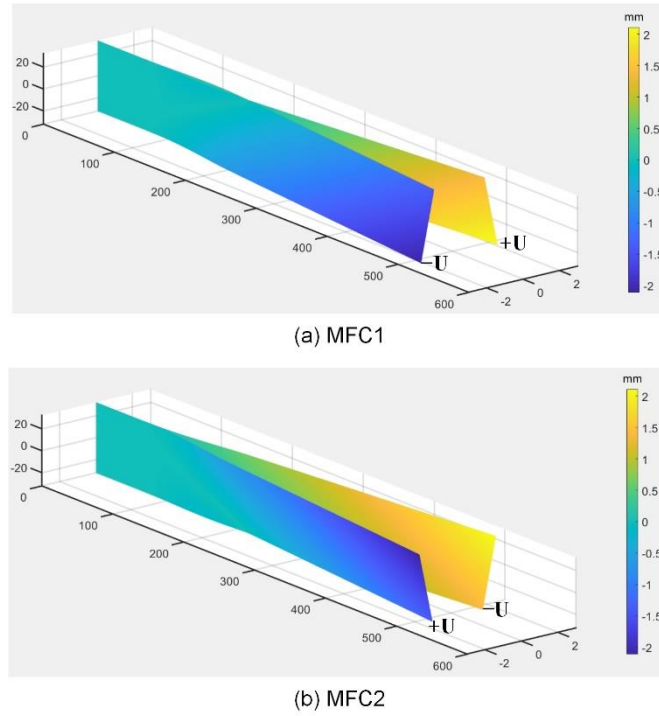


Figure 4. Deformation configuration of the substrate plate actuated by the single MFC. (a) Deformation configuration of the substrate plate actuated by the MFC1; (b) deformation configuration of the substrate plate actuated by the MFC2.

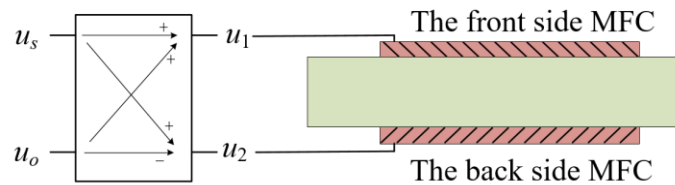


Figure 5. Voltage distributions for the two MFC actuators.

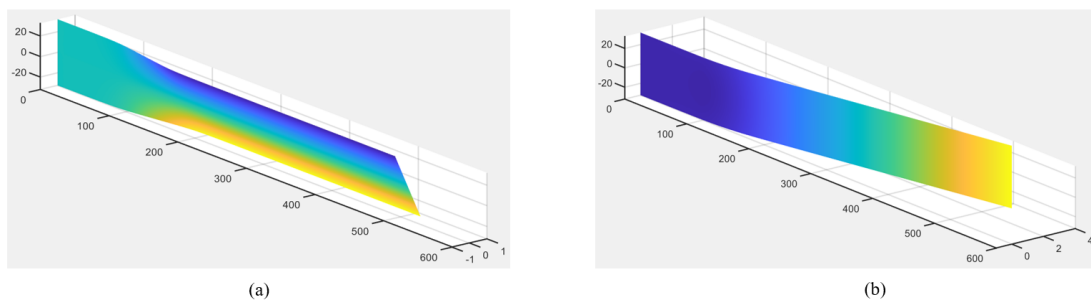


Figure 6. Bending (a) and twisting (b) shape control effect using different voltages for the actuators.

3. Experiment Implementation

3.1. Setup

An experimental setup was designed for validation according to the previous theoretical investigation, as shown in Figure 7. The base structure was a cantilever aluminum

plate, whose dimensional and material properties are listed in Table 1. Two identical MFC patches of type M8557-F1, which were produced by Smart Material Corp., Sarasota, FL, US [30], were glued to the front and backside surfaces of the base plate, respectively. The actuators were located 0.1 m from the plate root, as determined previously. A PCI-1721 DAQ card, which was produced by Advantech Co., Ltd., Kunshan, China, was used to convert the digital signals from the computer to the analog signals. Since the operational voltage of the MFCs ranged from -500 to 1500 V, a HVA 1500-2 high-voltage amplifier, which was produced by Physical Instruments Corp., Berlin, Germany, was used to supply the high voltage for the MFC. The elastic deformation of the plate was measured by two OPTEX-CDX-30A-type laser displacement sensors, which was produced by Guangzhou Optex Industrial Automation Control Equipment Co., Ltd. Guangzhou, China; thus, the twisting angle could be computed using Equation (6). The measured data obtained from the laser sensors were conducted using an ADAM-USB card, which was produced by Advantech Co., Ltd., Kunshan, China; thus the signals could be received by the computer. A computer integrated with MATLAB (which was produced by MathWorks Corp, Natick, MA, USA) and LabVIEW (which was produced by NI Corp, Austin, TX, USA) code was used to generate the voltage signals, receive the sensor signals, and implement the feedback closed-loop control laws.

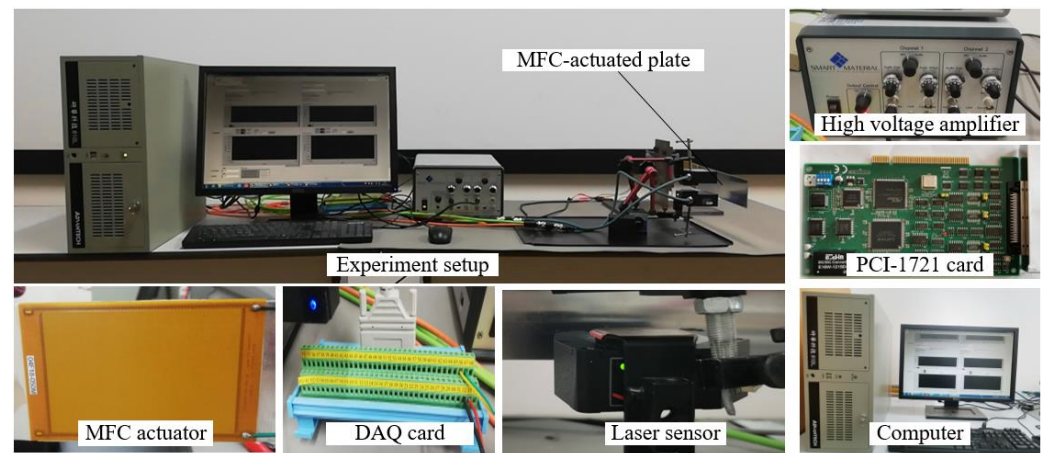


Figure 7. Experiment setup.

3.2. Modal Analysis

Before the active shape control tests, modal analysis was implemented first, for two purposes: (1) To investigate the dynamic characteristics of the compliant structure; and (2) to evaluate the influences of the bonded MFC actuators on the system. The modal frequencies and shapes can be determined by solving an eigenvalue problem of the FE model as follows:

$$\left[\mathbf{K} - \omega^2 \mathbf{M} \right] \Phi = 0 \quad (10)$$

where ω is the natural frequencies and Φ denotes the corresponding modal shapes. Figure 8 shows the structural modal shapes of the first six modes, including four bending modes and two torsional modes (third and sixth modes). It was observed that the bonded MFCs had relatively little influence on the modal shapes of the structure.

The frequencies were recognized in terms of the free vibration data of the plate using fast Fourier transform. Table 2 lists the natural frequencies for the first three bending modes and the first torsional mode with and without the MFC actuators. In general, the theoretical values were in good agreement with the experimental results. The results showed that, after adding MFC actuators, the frequencies of the first bending and first torsional modes increased, while the frequencies of the second and third bending modes decreased. Note that the influences of piezoelectric actuators depend on many issues, including the size, position, and fiber orientation of anisotropic piezocomposite materials.

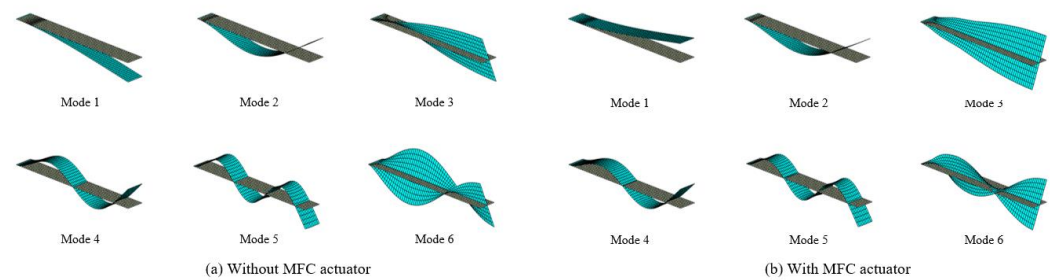


Figure 8. Structural modal shapes. (a) Structural modal shapes without MFC actuators; (b) structural modal shapes with MFC actuators.

Table 2. Natural frequencies of the structure with and without MFCs (Hz).

Mode	Without MFC			With MFCs		
	FEM	Experiment	Error	FEM	Experiment	Error
1st (bending)	3.34	3.27	2.14%	3.50	3.54	−1.13%
2nd (bending)	20.89	20.53	1.75%	19.57	19.51	0.30%
3rd (torsional)	49.90	46.63	5.80%	53.30	52.89	7.80%
4th (bending)	58.59	58.17	0.72%	54.40	57.45	−5.30%

3.3. Control Ability

In this study, the control ability of the MFCs in unimorph and bimorph was tested experimentally through static deformation analysis. To this end, the experimental steady-state deflection was obtained by directly applying a certain constant voltage for the MFC and recorded after a relative long time.

(a) Using single MFC

The elastic deflections of the two measurement points (i.e., w_{P_1} , w_{P_2}) under the single MFC are given in Figure 9. It can be observed that using a single MFC, both bending and twisting deformation were produced due to the off-line PZT fiber orientation. Moreover, as previously noted, the deflection amplitude of the lower-point P_2 produced by the MFC1 actuator was larger than the upper point P_1 , i.e., $|w_{P_1, \text{MFC1}}| < |w_{P_2, \text{MFC1}}|$ for both positive and negative voltages. Conversely, the deflections produced by the MFC2 showed the opposite trend, i.e., $|w_{P_1, \text{MFC2}}| > |w_{P_2, \text{MFC2}}|$. That is to say, the remarker given by Equation (7) and Figure 4 was verified by experiments. However, it can be observed that the actuation abilities of the two actuators were not identical, since the deflection amplitude generated by the MFC1 is larger than the MFC2. This deviation was induced by a variety of uncertainties and errors that are discussed in Section 3.4. That is to say, the theoretical remarker given by Equation (8) was not strictly met in the experiments.

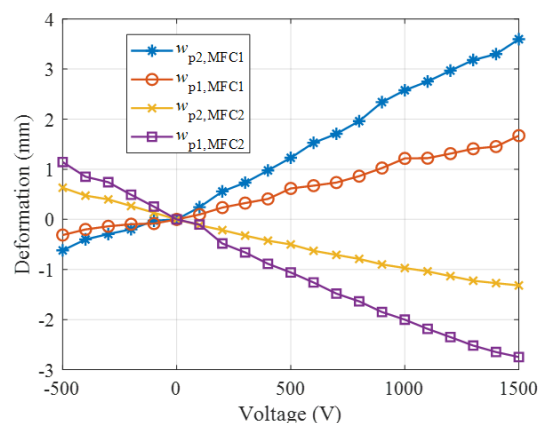


Figure 9. Deflection of the measurement points using a single MFC actuator.

(b) Using bimorph MFCs

The deflections of the plate under the actuation of the bimorph MFCs using the same and opposite voltages are shown in Figure 10, respectively. The x -axis in Figure 10b is labeled by the voltage of the MFC1, i.e., u_1 , so the corresponding voltage of the MFC2 is $u_2 = -u_1$. Because of the asymmetrical operation voltages (i.e., $-500\sim 1500$ V) for the MFCs, the operation voltage range is $-500\sim 1500$ V for the same sign; however, it is $-500\sim 500$ V for the opposite sign. It can be observed that the deflection amplitudes of the two points were generally equal; the deflection directions are opposite in Figure 10a (i.e., twisting deformation) and the same in Figure 10b (i.e., bending deformation), respectively. Moreover, the deflection amplitudes $|w_{p1}|$ and $|w_{p2}|$, which should be identical in terms of FE analysis, were still not the same in the two experimental cases. The above experiments imply that bending and twisting shape control can be qualitatively realized as theoretically predicted; however, they cannot be implemented with high control accuracy through an open-loop control approach alone.

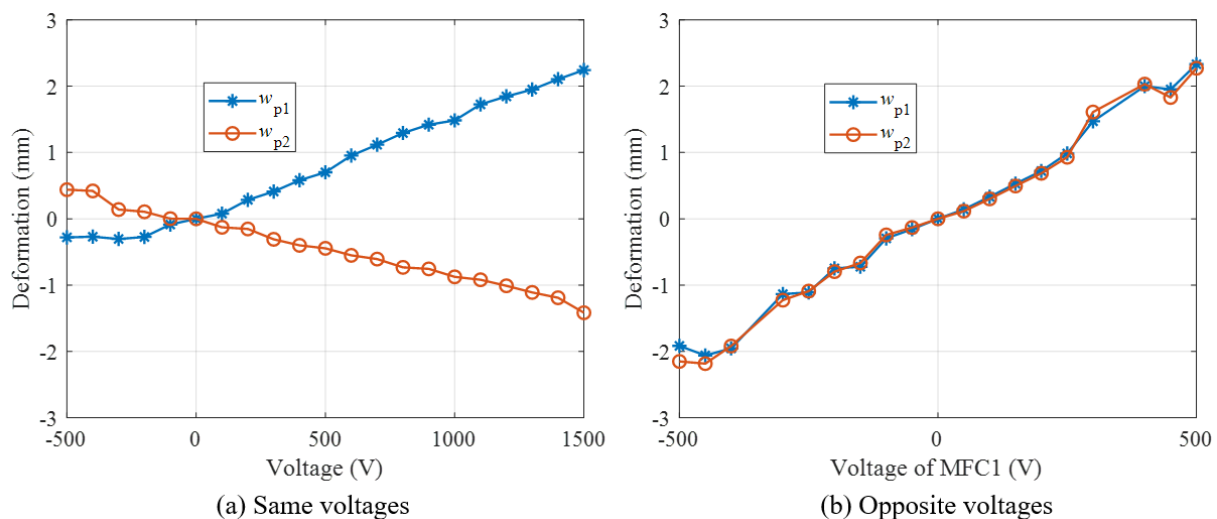


Figure 10. Deflection of the measurement points using bimorph MFC actuators. (a) Deflection of the measurement points using bimorph MFC actuators under the same voltages; (b) deflection of the measurement points using bimorph MFC actuators under the opposite voltages.

3.4. Uncertainty Analysis

The above experimental results demonstrate the independent bending/twisting shape control resulting from the use of MFCs in an antisymmetric angle-ply bimorph configuration. However, the open shape control accuracy is generally low due to a variety of uncertainties and nonlinearities.

Firstly, the shape control accuracy is also influenced by the non-uniform distribution of the substrate material of the plate, which is assumed as an isotropic aluminum plate in FE modeling. This non-uniform distribution induces changes in both the bending and torsional stiffness properties. Secondly, the MFC layer and the substrate plate are glued by using epoxy. Thus, the thickness and distribution of the epoxy layer also affect the actuation effect of the MFCs, especially the synchronization of the two actuators. Furthermore, the actuation performance is heavily affected by the nonlinearities of the MFCs, including hysteresis, creep, and varied piezoelectric coefficients [30]. Hysteresis and creep effects are the intrinsic nonlinear characteristics of piezoelectric actuators and can significantly affect the control performance [46], as shown in Figure 11. The hysteresis exhibited at a given time depends on the present input and the operational history of the system. Creep is related to the drift effect of output displacement with a constant applied voltage over extended periods. Furthermore, the piezoelectric coefficients of MFCs are also varied, depending on the situation; an example of this is the d_{33} and d_{31} piezoelectric constants in

high electric field intensity compared with low field intensity [30]. Furthermore, the shape control accuracy is also affected by the placement of wires, external disturbance, and so on.

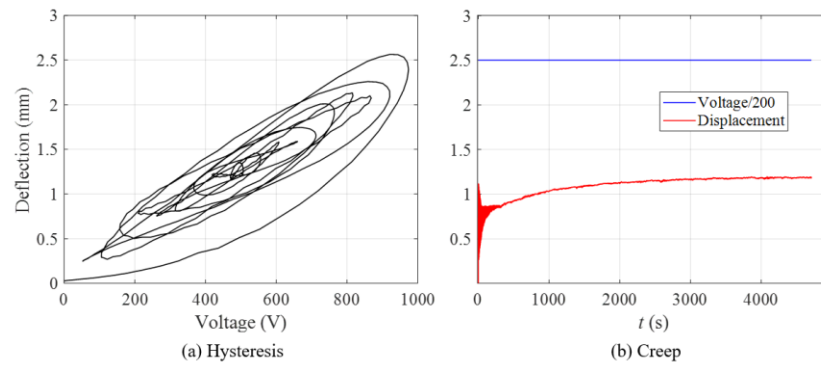


Figure 11. Hysteresis and creep effects of the MFC actuator. (a) Hysteresis effect of the MFC actuator; (b) creep effect of the MFC actuator.

Because of the above uncertainties and nonlinearities, accurate bending/twisting shape control cannot be ensured in experiments by using the voltage values estimated by the linear FE simulation. Some feedforward control schemes can be implemented to reduce or cancel out unwanted issues. For example, a feedforward inverse compensation control can be designed to cancel out the hysteresis and creep nonlinearities of MFCs in terms of a phenomenon-based model and experimental data [32]. However, it is still a difficult task to perform open-loop control given all the undesired effects. Therefore, a feedback control scheme is necessary to realize accurate bending/twisting shape control. It is easy to design a shape control law for a single-input–single-output (SISO) system, such as the bending shape control of a plate using M8528-P1-type MFCs in our previous study [47]. However, the plant in this study constitutes a two-input–two-output system, and the key point is how to design the control law to achieve both independent and coupled bending/twisting shape control.

4. Closed-Loop Multi-Mode Shape Control System

4.1. Feedback Control Law

To achieve the synthetic control of bending and twisting shape, the structural deformations are organized as follows:

$$\begin{aligned} B &= \frac{w_{p_1} + w_{p_2}}{2} \\ T &= \frac{w_{p_1} - w_{p_2}}{2} \end{aligned} \tag{11}$$

where B and T denote the bending and twisting components in the deformation, respectively. On the other hand, the deflections of the two points can also be represented by the components, i.e., $w_{p_1} = B + T$, $w_{p_2} = B - T$.

Hence, the shape control error can be given as

$$\begin{aligned} \Delta B &= B - B_d = \frac{\Delta w_{p_1} + \Delta w_{p_2}}{2} \\ \Delta T &= T - T_d = \frac{\Delta w_{p_1} - \Delta w_{p_2}}{2} \end{aligned} \tag{12}$$

where B_d and T_d denote the command bending and twisting requirements, respectively.

To adjust the shape control error, a feedback control law is designed as

$$\begin{aligned} \Delta u_s &= K_s \Delta T + K_{sB} \Delta B \\ \Delta u_p &= K_p \Delta B + K_{pT} \Delta T \end{aligned} \tag{13}$$

where Δu_s and Δu_p are the incremental voltage values for the same and the opposite components of the actuators in each time step, respectively. The values K_s and K_p denote

the primary control gains, which are designed according to ideal situations. The values K_{sB} and K_{pT} are used to compensate for the shape error associated with the uncertainties. Subsequently, the voltages for the two MFC actuators can be easily determined according to Equation (9).

4.2. Multi-Mode Shape Control Results

The multi-mode shape control was directly implemented based on the experiment by using B_c and T_c as the control requirements. According to Equation (11), the arbitrary deformation of the plate can be represented by a combination of bending and twisting components.

The pure twisting shape control results obtained by using $T_c = 0.8$ and $B_c = 0$ as the objectives are shown in Figure 12. Figure 12a gives the deflection histories of the two measurement points, i.e., w_{p1} and w_{p2} , which demonstrate that the same deformation amplitudes with opposite directions were achieved. The time histories of B and T shown in Figure 12b demonstrate that the pure twisting deformation of the plate was achieved, while the bending deformation was maintained at zero. It can be observed that the shape control accuracy was greatly improved, especially compared with the previous open-loop results. Figure 12c shows the time histories of the voltages for the two MFC actuators. It can be observed that the two voltages did not converge to the same value in terms of the ideal situation. Due to the influences of the creep effect, the voltages slowly varied with time. Furthermore, the deformations converged to the desired values. Such voltage profiles are difficult to determine by feedforward control due to complex uncertainties. The results again prove the necessity of closed-loop control in high-precision shape control.

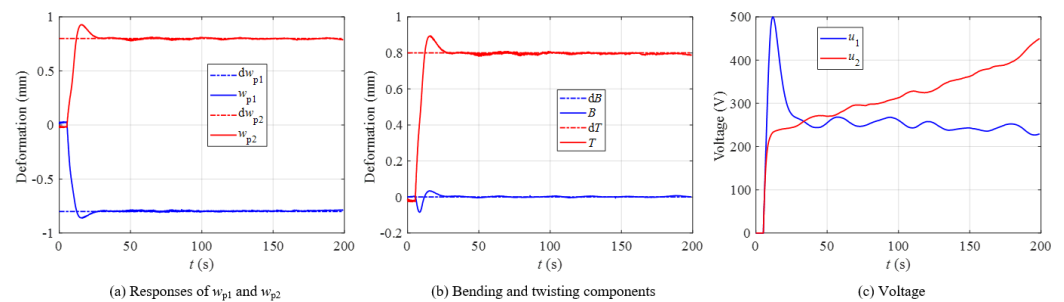


Figure 12. Pure twisting shape control performance. (a) The deflection histories of the two measurement points; (b) the time histories of B and T ; (c) the time histories of the voltages for the two MFC actuators.

Similarly, Figure 13 shows the pure bending shape control results obtained by using $T_c = 0$ and $B_c = 0.8$ as the objectives. The displacement of the two measuring points was consistent, without producing twisting deformation. The voltage profiles of the MFC1 and MFC2 were generally opposite to each other, as theoretically predicted; however, they still varied with time to resist the uncertainties and nonlinearities.

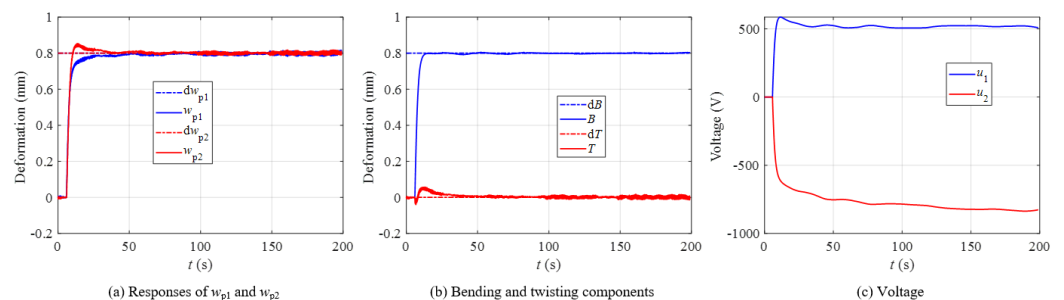


Figure 13. Pure bending shape control performance. (a) The deflection histories of the two measurement points; (b) the time histories of B and T ; (c) the time histories of the voltages for the two MFC actuators.

Finally, the coupled bending/twisting shape control (or arbitrary shape control) results are presented by using $T_c = 0.3$ and $B_c = 0.8$ as the objectives, as shown in Figure 14. It can be observed that both the bending and twisting deformations reached the command values with high shape accuracy. The two voltage values were adjusted in time according to the feedback control law to achieve arbitrary deformation. The trend in the voltage profiles can also be explained by Figures 12 and 13. The above results imply that independent bending and twisting shape control with improved shape accuracy was achieved by employing the multi-mode feedback control approach.

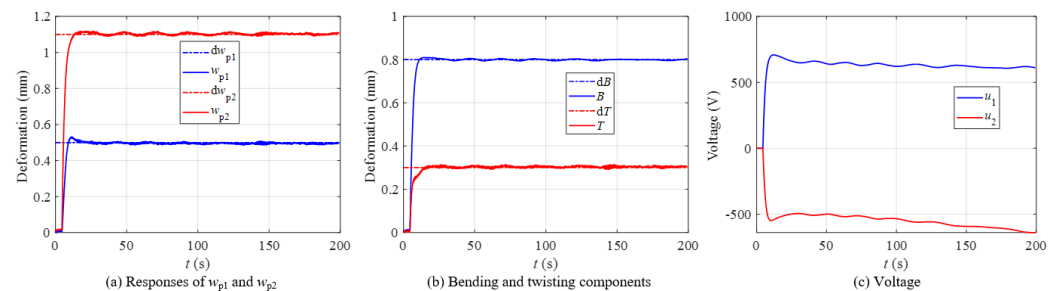


Figure 14. Arbitrary shape control performance. (a) The deflection histories of the two measurement points; (b) the time histories of B and T ; (c) the time histories of the voltages for the two MFC actuators.

5. Conclusions

In this paper, the multi-mode shape control of piezo-actuated compliant morphing structures was achieved in both theoretical and experimental ways. Independent and coupled bending/twisting shape control of a plate structure was achieved by using F1-type MFCs in an antisymmetric angle-ply bimorph configuration. The optimal locations of the MFC actuators were determined by comprehensively considering the control of the bending and twisting deformations. The experimental tests implied that the shape control accuracy was heavily reduced due to various uncertainties and nonlinearities, including hysteresis and the creep effect of the actuators, model errors, and external disturbances. A multi-mode feedback control law was designed to cancel out the shape error. The experimental results implied that synthetic (independent and coupled) bending and twisting shape control with improved shape accuracy was achieved by employing the multi-mode feedback control approach.

Author Contributions: Conceptualization, X.W.; Data curation, X.H.; Formal analysis, C.H.; Funding acquisition, X.W.; Investigation, X.H.; Methodology, X.W. and W.Z.; Software, X.H. and C.H.; Supervision, W.Z.; Writing—original draft, X.W.; Writing—review & editing, W.Z. All authors have read and agreed to the published version of the manuscript.

Funding: This research was funded by the National Natural Science Foundation of China (11872381, 12102096) and the Guangdong Basic and Applied Basic Research Foundation (2019A1515010859).

Institutional Review Board Statement: Not applicable.

Informed Consent Statement: Not applicable.

Data Availability Statement: Not applicable.

Acknowledgments: The author would like to thank the reviewers and the editors for their valuable comments and constructive suggestions that helped to improve the paper significantly.

Conflicts of Interest: The authors declare no conflict of interest.

References

1. Barbarino, S.; Bilgen, O.; Ajaj, R.M.; Friswell, M.I.; Inman, D.J. A review of morphing aircraft. *J. Intell. Mater. Syst. Struct.* **2011**, *22*, 823–877. [\[CrossRef\]](#)
2. Sun, J.; Guan, Q.; Liu, Y.; Leng, J. Morphing aircraft based on smart materials and structures: A state-of-the-art review. *J. Intell. Mater. Syst. Struct.* **2016**, *27*, 2289–2312. [\[CrossRef\]](#)

3. Baier, H.; Datashvili, L. Active and morphing aerospace structures—A synthesis between advanced materials, structures and mechanisms. *Int. J. Aeronaut. Space Sci.* **2011**, *12*, 225–240. [[CrossRef](#)]
4. Giurgiutiu, V. Review of smart-materials actuation solutions for aeroelastic and vibration control. *J. Intell. Mater. Syst. Struct.* **2000**, *11*, 525–544. [[CrossRef](#)]
5. Ferreira, A.D.B.L.; Nóvoa, P.R.O.; Marques, A.T. Multifunctional material systems: A state-of-the-art review. *Compos. Struct.* **2016**, *151*, 3–35. [[CrossRef](#)]
6. Bradford, S.C.; Agnes, G.S.; Ohara, C.M.; Green, J.J.; Shi, F.; Zhou, H. Controlling wavefront in lightweight active reflector systems using piezocomposite actuator arrays. In Proceedings of the 54th AIAA/ASME/ASCE/AHS/ASC Structures, Structural Dynamics and Materials Conference, Boston, MA, USA, 8–11 April 2013; AIAA: Reston, VA, USA, 2013.
7. Shao, S.; Song, S.; Xu, M.; Jiang, W. Mechanically reconfigurable reflector for future smart space antenna application. *Smart Mater. Struct.* **2018**, *27*, 095014. [[CrossRef](#)]
8. Bilgen, O.; Kochersberger, K.B.; Inman, D.J.; Ohanian, O.J. Novel, Bidirectional, Variable-Camber Airfoil via Macro-Fiber Composite Actuators. *J. Aircr.* **2010**, *47*, 303–314. [[CrossRef](#)]
9. Echter, M.A.; Silver, M.J.; D’Elia, E.; Peterson, M.E. Recent Developments in Precision High Strain Composite Hinges for Deployable Space Telescopes. In Proceedings of the 2018 AIAA Spacecraft Structures Conference, Kissimmee, FL, USA, 8–12 January 2018; p. 14.
10. Hill, J.; Wang, K.W.; Fang, H. Advances of Surface Control Methodologies for Flexible Space Reflectors. *J. Spacecr. Rocket.* **2013**, *50*, 816–828. [[CrossRef](#)]
11. Wang, Z.; Li, T.; Cao, Y. Active shape adjustment of cable net structures with PZT actuators. *Aerosp. Sci. Technol.* **2013**, *26*, 160–168. [[CrossRef](#)]
12. Song, X.; Tan, S.; Wang, E.; Wu, S.; Wu, Z. Active shape control of an antenna reflector using piezoelectric actuators. *J. Intell. Mater. Syst. Struct.* **2019**, *30*, 2733–2747. [[CrossRef](#)]
13. Hiroaki, T.; Sakamoto, H.; Inagaki, A.; Ishimura, K.; Doi, A.; Kono, Y.; Kuratomi, T. Development of a smart reconfigurable reflector prototype for an extremely high-frequency antenna. *J. Intell. Mater. Syst. Struct.* **2016**, *27*, 764–773. [[CrossRef](#)]
14. Sakamoto, H.; Tanaka, H.; Ishimura, K.; Doi, A.; Kono, Y.; Matsumoto, N. Shape-control experiment of space reconfigurable reflector using antenna reception power. In Proceedings of the 3rd AIAA Spacecraft Structures Conference, San Diego, CA, USA, 4–8 January 2016; p. 0703.
15. Monner, H.P.; Riemenschneider, J.; Opitz, S.; Schulz, M. Development of active twist rotors at the German Aerospace Center (DLR). In Proceedings of the 52nd AIAA/ASME/ASCE/AHS/ASC Structures, Structural Dynamics and Materials Conference, Denver, CO, USA, 4–7 April 2011; AIAA: Reston, VA, USA, 2011.
16. Riemenschneider, J.; Keye, S.; Wierach, P.; Mercier Des Rochettes, H. Overview of the common DLR/ONERA project “Active Twist Blade” (ATB). In Proceedings of the 30th European Rotorcraft Forum, Marseilles, France, Confederation of European Aerospace Societies, Brussels, Belgium, 14–16 September 2005; pp. 273–281.
17. Li, M.; Chen, W.; Guan, D.; Li, W. Experimental validation of improving aircraft rolling power using piezoelectric actuators. *Chin. J. Aeronaut.* **2005**, *18*, 108–115. [[CrossRef](#)]
18. Bilgen, O.; Kochersberger, K.; Diggs, E.C.; Kurdila, A.J.; Inman, D.J. Morphing wing micro-air-vehicles via macro-fiber-composite actuators. In Proceedings of the 48th AIAA/ASME/ASCE/AHS/ASC Structures, Structural Dynamics, and Materials Conference, Honolulu, HI, USA, 23–26 April 2007; AIAA: Reston, VA, USA, 2007; pp. 1005–1020.
19. Bilgen, O.; Friswell, M.I. Piezoceramic composite actuators for a solid-state variable-camber wing. *J. Intell. Mater. Syst. Struct.* **2014**, *25*, 806–817. [[CrossRef](#)]
20. LaCroix, B.W.; Ifju, P.G. Aeroelastic model for macrofiber composite actuators on micro air vehicles. *J. Aircr.* **2016**, *54*, 199–208. [[CrossRef](#)]
21. Molinari, G.; Arrieta, A.F.; Ermanni, P. Aero-Structural Optimization of Three-Dimensional Adaptive Wings with Embedded Smart Actuators. *AIAA J.* **2014**, *52*, 1940–1951. [[CrossRef](#)]
22. Usher, T.D.; Ulibarri, K.R., Jr.; Camargo, G.S. Piezoelectric microfiber composite actuators for morphing wings. *ISRN Mater. Sci.* **2013**, *2013*, 1–9. [[CrossRef](#)]
23. Wetherhold, R.C.; Aldraihem, O.J. Bending and twisting vibration control of flexible structures using piezoelectric materials. *Shock. Vib. Dig.* **2001**, *33*, 187–197. [[CrossRef](#)]
24. Ray, M.C.; Reddy, J.N. Active damping of laminated cylindrical shells conveying fluid using 1–3 piezoelectric composites. *Compos. Struct.* **2013**, *98*, 261–271. [[CrossRef](#)]
25. Smith, W.A.; Auld, B.A. Modeling 1–3 composite piezoelectrics: Thickness-mode oscillations. *IEEE Trans. Ultrason. Ferroelectr. Freq. Control* **1991**, *38*, 40–47. [[CrossRef](#)]
26. Choi, S.C.; Park, J.S.; Kim, J.H. Vibration control of pre-twisted rotating composite thin-walled beams with piezoelectric fiber composites. *J. Sound Vib.* **2007**, *300*, 176–196. [[CrossRef](#)]
27. Bent, A.A.; Hagood, N.W.; Rodgers, J.P. Anisotropic actuation with piezoelectric fiber composites. *J. Intell. Mater. Syst. Struct.* **1995**, *6*, 338–349. [[CrossRef](#)]
28. Kwak, S.K.; Yedavalli, R.K. New modeling and control design techniques for smart deformable aircraft structures. *J. Guid. Control Dyn.* **2001**, *24*, 805–815. [[CrossRef](#)]

29. Wang, X.; Zhou, W.; Wu, Z.; Xing, J. Tracking control system design for roll maneuver via active wings using macro fiber composites. In Proceedings of the AIAA Modeling and Simulation Technologies Conference, Washington, DC, USA, 9–13 January 2017; AIAA: Reston, VA, USA, 2016.
30. Smart-Material-Corporation. 2022. Available online: <https://www.smart-material.com/MFC-product-mainV2.html> (accessed on 30 March 2022).
31. Bilgen, O.; Kochersberger, K.B.; Inman, D.J.; Ohanian, I.O.J. Lightweight high voltage electronic circuits for piezoelectric composite actuators. *J. Intell. Mater. Syst. Struct.* **2010**, *21*, 1417–1426. [[CrossRef](#)]
32. Schröck, J.; Meurer, T.; Kugi, A. Control of a flexible beam actuated by macro-fiber composite patches—Part II: Hysteresis and creep compensation, experimental results. *Smart Mater. Struct.* **2011**, *20*, 015016. [[CrossRef](#)]
33. Wickramasinghe, V.; Chen, Y.; Martinez, M.; Wong, F.; Kernaghan, R. Design and verification of a smart wing for an extreme-agility micro-air-vehicle. *Smart Mater. Struct.* **2011**, *20*, 125007. [[CrossRef](#)]
34. Ohanian, O.J.; David, B.M.; Taylor, S.L.; Kochersberger, K.B.; Probst, T.; Gelhausen, P.A. Piezoelectric morphing versus servo-actuated MAV control surfaces, part II: Flight testing. In Proceedings of the 51st AIAA Aerospace Sciences Meeting Including the New Horizons Forum and Aerospace Exposition, Grapevine, TX, USA, 7–10 January 2013; AIAA: Reston, VA, USA, 2013.
35. Wang, X.; Zhou, W.; Wu, Z. Feedback tracking control for dynamic morphing of piezocomposite actuated flexible wings. *J. Sound Vib.* **2018**, *416*, 17–28. [[CrossRef](#)]
36. Wang, X.; Zhou, W.; Xun, G.; Wu, Z. Dynamic shape control of piezocomposite-actuated morphing wings with vibration suppression. *J. Intell. Mater. Syst. Struct.* **2018**, *29*, 358–370. [[CrossRef](#)]
37. Zhou, W.; Wang, X.; Qian, W.; Wu, W. Optimization of Locations and Fiber Orientations of Piezocomposite Actuators on Flexible Wings for Aeroelastic Control. *J. Aerosp. Eng.* **2019**, *32*, 04019056. [[CrossRef](#)]
38. Wang, X.; Zhou, W.; Wu, Z.; Wu, W. Optimal unimorph and bimorph configurations of piezocomposite actuators for bending and twisting vibration control of plate structures. *J. Intell. Mater. Syst. Struct.* **2018**, *29*, 1685–1696. [[CrossRef](#)]
39. Wang, X.; Zhou, W.; Wu, Z.; Zhang, X. Integrated design of laminated composite structures with piezocomposite actuators for active shape control. *Compos. Struct.* **2019**, *215*, 166–177. [[CrossRef](#)]
40. Williams, R.B.; Grimsley, B.W.; Inman, D.J.; Wilkie, W.K. Manufacturing and mechanics-based characterization of macro fiber composite actuators. In Proceedings of the ASME 2002 International Mechanical Engineering Congress and Exposition, New Orleans, LA, USA, 17–22 November 2002; ASME: New York, NY, USA, 2002; pp. 79–89.
41. Zhang, S.-Q.; Li, Y.-X.; Schmidt, R. Modeling and simulation of macro-fiber composite layered smart structures. *Compos. Struct.* **2015**, *126*, 89–100. [[CrossRef](#)]
42. Zhang, S.-Q.; Zhao, G.-Z.; Rao, M.N.; Schmidt, R.; Yu, Y.-J. A review on modeling techniques of piezoelectric integrated plates and shells. *J. Intell. Mater. Syst. Struct.* **2019**, *30*, 1133–1147. [[CrossRef](#)]
43. Chee, C.Y.K.; Tong, L.Y.; Steven, G.P. A review on the modelling of piezoelectric sensors and actuators incorporated in intelligent structures. *J. Intell. Mater. Syst. Struct.* **1998**, *9*, 3–19. [[CrossRef](#)]
44. Gupta, V.; Sharma, M.; Thakur, N. Optimization criteria for optimal placement of piezoelectric sensors and actuators on a smart structure: A technical review. *J. Intell. Mater. Syst. Struct.* **2010**, *21*, 1227–1243. [[CrossRef](#)]
45. Frecker, M.I. Recent advances in optimization of smart structures and actuators. *J. Intell. Mater. Syst. Struct.* **2003**, *14*, 207–216. [[CrossRef](#)]
46. Cao, Y.; Chen, X.B. A Survey of Modeling and Control Issues for Piezo-Electric Actuators. *J. Dyn. Syst. Meas. Control Trans. ASME* **2015**, *137*, 010101. [[CrossRef](#)]
47. Wang, X.; Zhou, W.; Zhang, Z.; Jiang, J.; Wu, Z. Theoretical and experimental investigations on modified LQ terminal control scheme of piezo-actuated compliant structures in finite time. *J. Sound Vib.* **2021**, *491*, 115762. [[CrossRef](#)]